A Study of Radio Frequency Interference in the Space-to-Earth Exploration Allocation at L-Band

J. Eric Belz[1], Bryan L. Huneycutt[2], Michael W. Spencer[3]
Jet Propulsion Laboratory, California Institute of Technology
4800 Oak Grove Drive
Pasadena, CA 91109-8099
1: (818)-354-1220, eric.belz@jpl.nasa.gov 2: (818) 354-2646, Bryan.L.Huneycutt@jpl.nasa.gov 3: (818) 354-1175, Michael.W.Spencer@jpl.nasa.gov

Abstract—We report on ongoing studies of the anthropogenic radio frequency interference (RFI) in the L-band allocation for space-to-Earth exploration.[1,2] The studies are being conducted for the radar instrument on the proposed Soil Moisture Active/Passive (SMAP) mission. A review of the allocated emitters is presented, followed by analysis based on space-borne and airborne data collected from the PALSAR sensor and the UAVSAR sensor. We use these data to model the pulsed RFI environment for SMAP and to demonstrate that the baseline plans for RFI mitigation are technically sound.

TABLE OF CONTENTS

1. INTRODUCTION

The Proposed SMAP Mission

In 2007 the National Research Council completed its first decadal survey for Earth science to provide scientific direction for several US agencies, including NASA, NOAA, and the USGS [1]. This report identified several Earth-observing mission concepts based on L-band microwave sensors sensitive to observables such as ocean salinity, soil moisture, freeze-thaw state, topography and surface change. The frequency allocation for active space-borne Earth observation, 1215 –1300 MHz, is shared with radiolocation, space-to-earth radio-navigation, active space research, and amateur communication. Those users present significant sources of anthropogenic radio frequency interference (RFI) to be addressed at the top level of any L-band sensor system.

The proposed Soil Moisture Active/Passive (SMAP) Mission is currently scheduled to launch in late 2015 [2].

[1] 978-1-4244-7351-9/11/$26.00 ©2011 IEEE
[2] IEEEAC paper#1318, Version 1, Updated 2010:10:25

The science objectives of SMAP would provide frequent, global measurements of surface soil moisture and surface freeze/thaw state. These measurements would be used to enhance the understanding of water, energy, and carbon cycles, as well as improve weather and climate prediction. The key instrument requirements were determined by the SMAP science working group to be (1) dual-polarization (linear H and V) L-band passive radiometer measurements; (2) linear HH, VV and HV L-band radar measurements; and (3) a wide swath to ensure global three-day refresh time for these measurements (1000 km swath at the selected orbit altitude of 680 km).

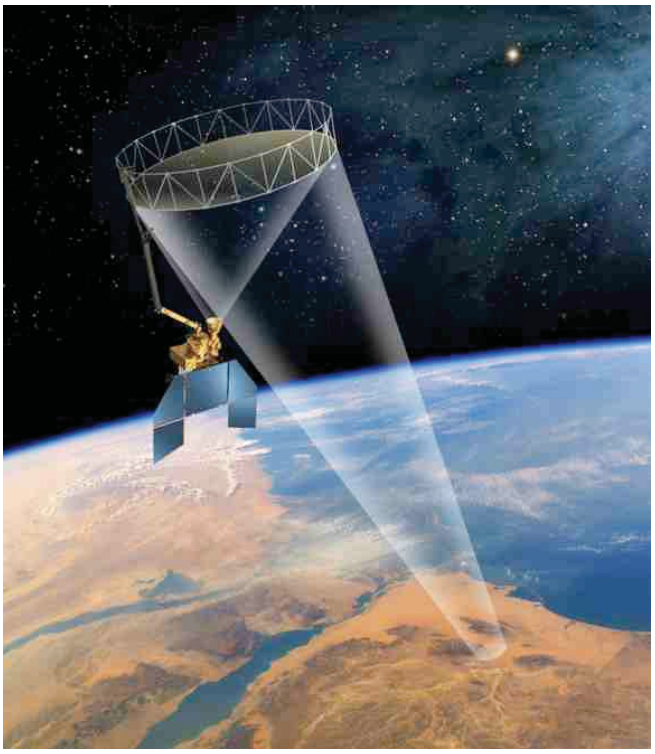

Figure 1 – Artist's rendition of SMAP in orbit.

To meet these requirements, a 6-meter, conically-scanning reflector antenna architecture was selected for the instrument design. The deployable mesh antenna is shared by both the radiometer and radar instruments by using a single L-band feed. The overall SMAP concept is shown in Figure 1 and illustrates the unique large rotating antenna. At the nominal SMAP altitude of 680 km, the reflector must

be rotated at a rate of 14.6 rpm to maintain contiguity (i.e., minimum overlap) of the measurements in the along-track direction. The baseline feed assembly design employs a single horn, capable of dual-polarization and dual frequency (radiometer frequency at 1410 MHz and the tunable radar frequencies from 1217.25 to 1297.75 MHz).

The high-resolution mode of SMAP would have 3 km resolution with a radiometric accuracy of 0.4 dB (K_p) in order to meet the mission's proposed science requirements. RFI poses a significant error source for that measurement, as an interference-to-signal ratio (ISR) of -10 dB may use the entire error budget. In order to understand and estimate the RFI environment, both UAVSAR [3] and ALOS/PALSAR [4] data have been used to observe RFI.

Method

This study uses both airborne and space-borne measurements; airborne data covering 1215-1300 MHz were collected with NASA/JPL's UAVSAR platform, while space-borne measurements use data from JAXA's ALOS/PALSAR instrument, which operates over a smaller bandwidth from 1254-1286 MHz.

The nominal operational plan for mitigating RFI in SMAP is to avoid it with frequency agility; nevertheless, RFI energy will still get into the data stream. Pulsed RFI will be detected via the increased power in the signal; those portions of the data will be excised and the formation of the synthetic aperture will proceed. Finally, the single look pixels will be combined into accurate radiometric science products.

The above plan is only feasible if the following hold:

(1) The number of range lines with RFI is small enough so that a synthetic aperture can be formed.
(2) Even though range-lines with RFI are removed, an accurate radiometric data product can still be formed.
(3) The total RFI power that falls below the detection threshold is not so large as to spoil the radiometric measurement.

The data are used to address these points as follows.

The PALSAR data are used to emulate the timing, bandwidth, and formation of SMAP's synthetic aperture in order to estimate the fraction of pixels that will be lost because of RFI. The PALSAR data are also used to model SMAP's high-resolution radiometric data product; we demonstrate a RFI removal algorithm to recover the radiometric measurement. Finally, we present and demonstrate a method to estimate pulsed RFI power for very small signals with noise-only data from UAVSAR.

2. The RFI Environment

The L-Band spectrum from 1215 – 1300 MHz is allocated to radio-navigation satellite service (RNSS) [5], radiolocation, and amateur communication [6], with the first two sources presenting significant interference to SMAP's planned signal. Preliminary modeling has shown that sources coupling into SMAP's side-lobes are significant, moreover SMAP's circle of visibility would have a diameter of nearly 6000 km, which can encompass all of the continental United States.

RNSS Systems

The RNSS systems in the 1215-1300 MHz band include those of the Global Navigation Satellite Systems (GNSS), the Satellite-Based Augmentation System (SBAS) and Regional Navigation Satellite Systems. The GNSS systems and band designations include the GLONASS (L2), Navstar Global Positioning System (GPS) (L2), Galileo (E6), Quasi-Zenith Satellite System (QZSS) (L2C and LEX), COMPASS (B3 and B3-A) as illustrated in Figure 2. The SBAS systems include those of the US Wide Area Augmentation System (WAAS). The Regional Navigation Satellite Systems include Inmarsat navigation networks and the Indian Regional Navigation Satellite System (IRNSS). These systems are being addressed in a separate study and are not considered further here.

Radiolocation Sources

Radiolocation sources at L-band are mainly long range air route surveillance radars and military air defense radars. These radars typically have a range of roughly 200 nautical miles, and emitters are spaced accordingly. Systems are typically placed throughout a region or along its perimeter (as shown in Figure 3).

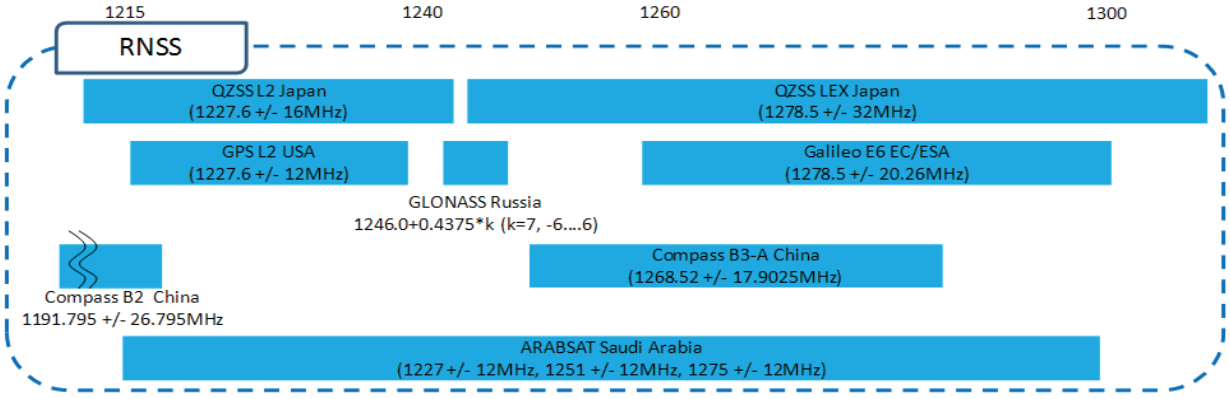

Figure 2 – Illustration of Frequency Band Ranges of RNSS Systems in the 1215-1300 MHz Band [7].

Figure 3 –ARSR-4 radar locations, as taken from Ref [8]. Sites not shown are Guantanamo Bay, Cuba, Santa Rosa, Guam, and Mount Kaala, HI. The two test and evaluation sites (shown in green) include Watford City, ND and Makah, WA.

These radars are pulsed, and typically have a bandwidth comparable to that planned for SMAP. Many of the signals in the PALSAR data over the United States match the known characteristics of these radars, and data over Europe, Asia, South America, and Africa show that similar systems are in use.

The majority of RFI measured is from pulsed system, though some continuous wave (CW) systems are presented in Appendix I.

3. PALSAR RFI OBSERVATIONS

The PALSAR Mission

The PALSAR mission was launched onboard the ALOS spacecraft [9] on January 24, 2006 in a sun-synchronous orbit with an altitude of 692 km (at the equator) and an orbital inclination of 98.16 degrees. PALSAR comprises a polarimetric L-band radar SAR system with several modes of operation. The center frequency is 1270 MHz, and the transmit and receive bandwidths are 28 MHz and 32 MHz, respectively. The orbit characteristics are similar to those projected for SMAP and the received frequencies range from 1254-1286 MHz, which covers 40% of the operating frequencies planned for SMAP. Moreover, the 32 MHz in phase/quadrature sample rate provides significant oversampling of the typical L-band radiolocation signals.

PALSAR's primary limitation as a model for SMAP is the antenna. Because PALSAR has a rectangular phased array patch antenna, the side-lobe structure differs significantly from that planned for SMAP; they are strongly peaked along the azimuth and elevation planes, while SMAP's side lobes would be far less pronounced. A secondary limitation is the limited dynamic range. The 5-bit ADC is easily saturated by large RFI signals, complicating spectral analysis because of clipping.

Data Summary

PALSAR data is publicly available from the Alaska Satellite Facility. The data presented here are taken from 363 data items from Chickasha, Ames, Huntsville, Bakersfield, Southern Ontario, New Zealand, Alaska, the Amazon, Saskatchewan, Qinghai, China, and Hong Kong. Each data item is typically 12-17 s of data, comprising about 35,000 range lines. In high-resolution mode, each range line is typically ~10,000 I-Q sample pairs spanning 322 μs, with about ~152 μs of dead time between radar pulses; that is, the system measures RFI with an average duty cycle of 68%.

PALSAR transmits a 27 μs pulse that is a 28 MHz linear down chirp. In the absence of RFI, the signal amplitude is roughly 3 sigma away from saturation, though the total power varies with the imaged scene. A typical echo with RFI is shown in Figure 4.

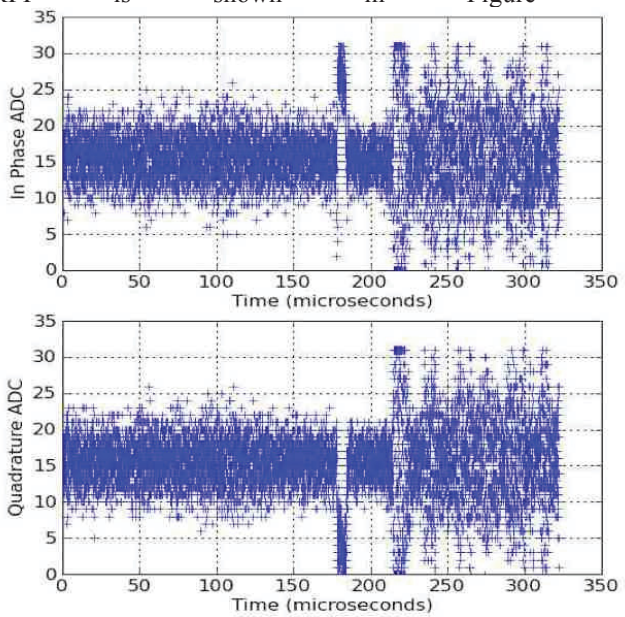

Figure 4 – A typical PALSAR range line with 2 RFI pulses. The top (bottom) plot show the in-phase (quadrature) ADC samples. At 180 μs there is a simple pulsed radar signal, and at 220 μs a chirped signal begins.

RFI Detection

RFI analysis is based on threshold detection, which is capable of detecting pulsed RFI signals. The detailed statistics of coherent radar measurements with RFI are presented in Appendix II. The formulae are essential for computing the probability of false alarm and the detection efficiency, both of which are required to estimate the systematic bias in a radiometric measurement.

Each receive channel in the SMAP system would operate

with a 1 MHz bandwidth that is tunable over 80 MHz. This is modeled with the PALSAR data by bandpass-filtering with 1 MHz bandwidth centered at 32 frequencies ranging from 1254.5 MHz to 1285.5 MHz, in 1 MHz intervals. For a single sub-band, each range-line becomes 322 range-samples taken at 1 MHz. RFI detection is then done at fixed range by comparing the total power to the median of neighboring range lines using a moving median filter with 101 elements. We evaluate the ratio of the measured power to the (moving) median power and set the RFI detection flag if the ratio exceeds a threshold of 4 standard deviations above the median.

After processing all sub-bands, each PALSAR data item is reduced to a series of RFI detection flags with 1 MHz frequency resolution and 1 μs time resolution, spanning ~15 seconds with a ~68% duty cycle. The total data processed represents over 4 billion samples at each frequency.

Modeling SMAP

SMAP is being designed with frequency agility in order to avoid RFI. SMAP's high-resolution raw data range lines would be composed of 250 range samples taken every microsecond, followed by 63 μs of dead time until the next pulse is received. One hundred twelve range lines constitute a single synthetic aperture. The baseline plan for RFI mitigation is to detect RFI in a range line and excise that portion of the range line before SAR image formation. Clearly, removing too many range lines from the data will spoil the formation of the aperture, preventing the recovery of sufficient data to generate the science product. A separate study to determine the effect of removing range lines on both the aperture formation and radiometric measurement is ongoing. Nevertheless, the PALSAR data can be used to estimate the raw data loss from RFI within the synthetic aperture.

The RFI sources would be quasi-regular with various pulse repetition frequencies asynchronous with SMAP's radar, so that a constant source will in general exhibit range walk as the SMAP system would observe it. A source or sources that may pulse many times during the 33 ms it would take SMAP to form a synthetic aperture will most likely appear in multiple range cells, and hence won't ruin the data for any single range/azimuth cell.

PALSAR data can be used to estimate this phenomenon by rearranging the PALSAR RFI detection flags to reflect the receive window timing planned for SMAP. Since they are sampled at the planned sample rate of SMAP (1 MHz), the procedure involves re-wrapping the data array according to the SMAP pulse repetition interval (3500 Hz). The data are then combined in both range and azimuth as if they were SMAP measurements; that is, range data are summed in 3 km (ground range) increments and 112 azimuth sample groups, representing a single look pixel at fixed range.

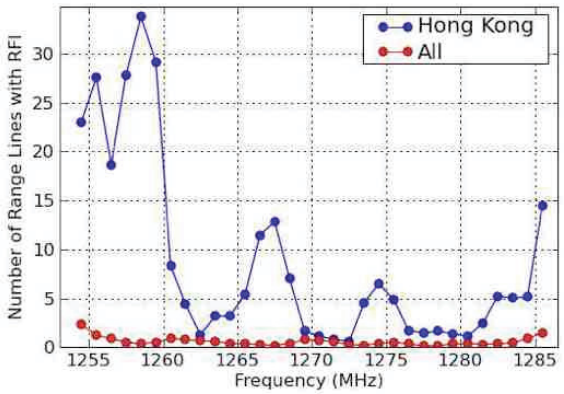

Figure 5 – The frequency dependence of RFI over the PALSAR's bandwidth, as measured by the number of range lines with detectable RFI in a simulated SMAP synthetic aperture. The red points are the average over 363 PALSAR data items, while the blue points are from the most heavily contaminated region (Hong Kong).

In our analysis, the number of range-lines with RFI detected in the pixel is counted at each frequency. The results provide an estimate of the expected RFI contamination of a SMAP synthetic aperture pixel at a given frequency and geographic location. Figure 5 provides an example of both the worst observed location (Hong Kong) and the global average. The figure shows that on average the RFI level is low enough that SMAP can meet it's science requirement at any frequency, though at some location frequency agility may be necessary.

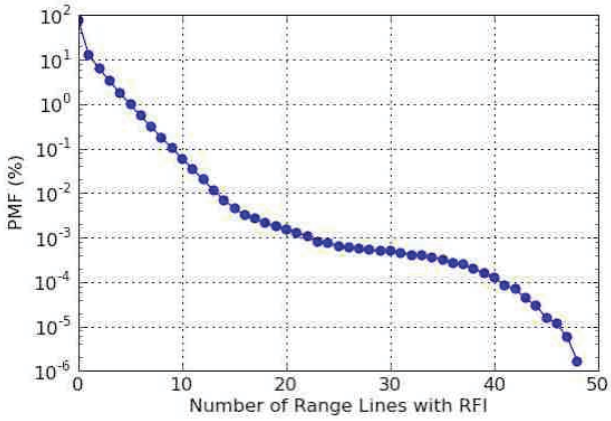

Figure 6 – Estimated probability distribution of RFI contamination of a SMAP synthetic aperture as measured by the number range lines with detectable RFI. 99.9% of the single-look pixels have less than 10 range lines with RFI.

The total processed data simulate 3.9 million SMAP single look pixels at each of 32 frequencies. Figure 6 shows the normalized histogram of range lines with detectable RFI and demonstrates that 74% of all the pixels have no detectable RFI and that a few pixels have over 40% of their range-lines

contaminated.

To better understand how the observed RFI could affect the delivery of data products, given that SMAP's planned operating frequency would be tunable, data from different locations are combined in several ways: all frequencies are averaged, the best frequency selection is made for each data item, or the worst frequency selection is made. With the assumption that apertures losing less than 10 range lines can be processed, the model shows that SMAP would be affected by RFI, but the requirement that 95% of the measurements be recovered would be met. Figure 7 illustrates the variation in data loss as a function maximum tolerable RFI contamination for each of these modeled cases.

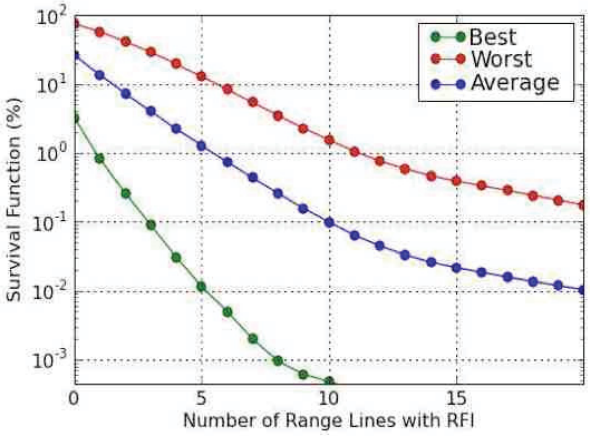

Figure 7 – The complementary cumulative distribution functions for RFI contamination of modeled SMAP synthetic apertures as measured by the number of range lines with RFI in a range-azimuth pixel. Since SMAP would have frequency agility, the data are shown for the best frequency choice (green), the worst frequency choice (red), and the average over the spectrum (blue). Data loss because of too many range lines wih RFI must remain below the magenta line (5%).

Range Line Excision and Radiometric Bias

In the baseline data processing methodology, when RFI is detected in the raw data, that range line is excised and replaced by the previous range line. However, this technique requires randomizing the phase of the copied range line with a random distribution determined by the statistics of the data. A test of this method was done using PALSAR data.

The PALSAR test used two data sets: one with RFI (Alaska) and one with very little (New Zealand). Each data set was sub-banded into 28 data sets with 1 MHz bandwidth. Unfocused SAR processing was done by range compressing and then coherently adding 73 range lines, which was chosen to match the synthetic aperture formation time of the SMAP design. The modeling of SMAP 3 km x 3 km pixels was done by incoherently averaging 13 μs of range data, representing the proper timing of SMAP slant-range data needed to span 3 km in ground range. In azimuth, 820 samples were taken because this is the time it takes PALSAR to travel 3 km. The resulting SMAP-like images are 26 x 37 pixels (range x azimuth).

The images were formed with and without the range-line substitution algorithm described previously. The RFI-free data from New Zealand were used to calibrate the frequency response in each of the 28 sub-bands.

The spectrum of the Alaska data with RFI is shown in Figure 8 and shows a series of ~1 MHz bandwidth RFI emitters separated by ~1 MHz of RFI-free spectrum.

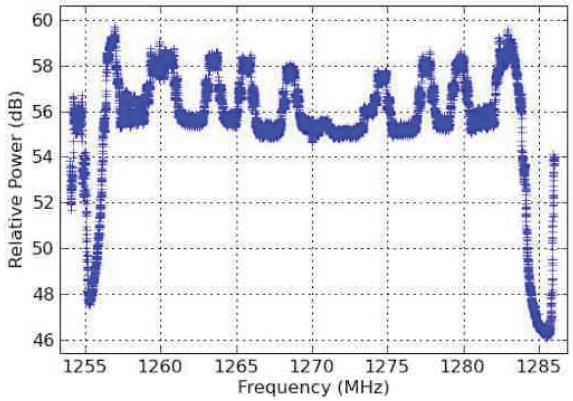

Figure 8 – Alaska PALSAR data set used to test the range line substitution algorithm. 1 MHz bandwidth RFI emitters are separated by 1 MHz of RFI-free signal.

Calibrating the power and integrating it in each of the sub-bands results in 11 sub-bands with significant RFI contamination and 17 sub-bands with little or no RFI. We use our range line excision technique in sub-bands with RFI and compare the results to the RFI-free sub-bands. Figure 9 shows the results of this analysis and demonstrates that the range line excision technique agrees well with measurements made in the RFI-free sub-bands.

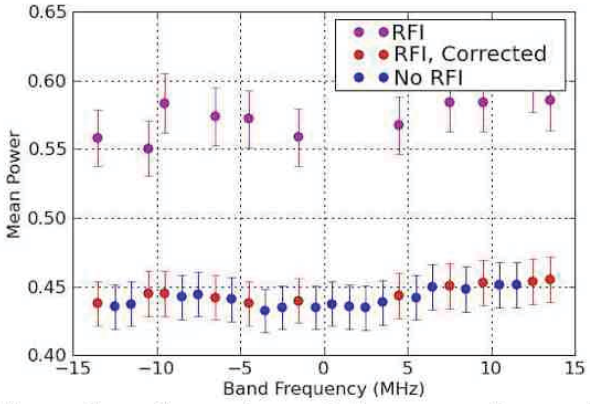

Figure 9 – Comparison of the range line excision technique with analysis in RFI-free sub-bands. The technique produces results that agree well with RFI-free data.

Finally, we evaluate the efficacy of the RFI correction algorithm by computing the variation in each simulated 3 km pixel for each sub-band using the average of the 17 RFI-free pixels at each point in the image. Figure 10 compares the data before and after the correction is applied. The results are summarized in Table I. Without correction the bias is significantly larger than the 0.4 dB budget, while after correction it is well within requirements.

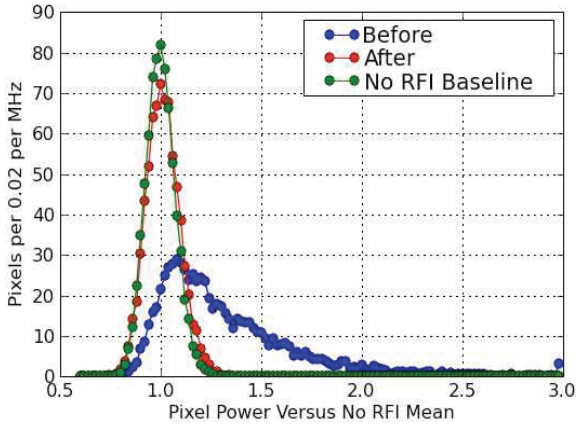

Figure 10 – The green points are a normalized histogram of the ratio of the measured power to the expected power for sub-bands with no RFI. The blue points are for sub-bands with RFI, which become the red points are after the RFI has been removed.

Table 1. Summary of Radiometric Measurements

	Bias	Standard Deviation
No RFI Sub-Bands	0 dB	0.076
Sub-Bands with RFI	1.3 dB	0.38
Sub-Bands with RFI after range line substitution	0.076dB	0.086

4. UAVSAR DATA

The UAVSAR system is an airborne L-band synthetic aperture radar system designed for repeat track interferometry in support of Earth science applications. It is deployed on a NASA Grumman Gulfstream III jet. The system supports full quad-polarization; nominally it transmits an 80 MHz chirp and has a receive bandwidth of 90 MHz with 12-bit ADC sampling at 180 MHz. In support of SMAP's RFI study, "noise-only" data have been collected at multiple sites.

Several flights in Alaska were conducted near long-range radar installations. Figure 11 shows a representative spectrum from a flight line. The spectrum represents roughly 500,000 pulses spanning about 30 minutes.

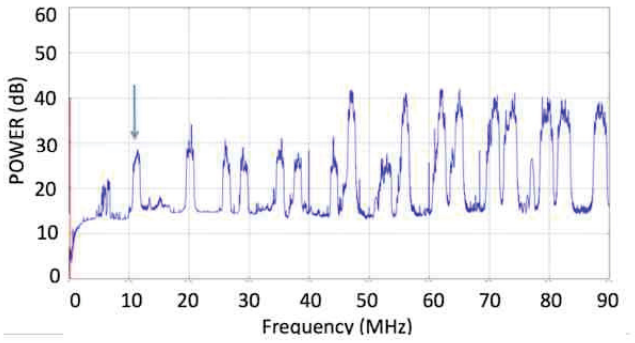

Figure 11 – A representative spectrum from a UAVSAR flight in Alaska. The source shown by the arrow is analyzed (relative to 1215 MHz).

The spectrum shows multiple high power emitters. This analysis focuses on a 1-MHz band centered on the source near 1226 MHz. Figure 12 shows the total power per range-line in the bandwidth analyzed. The figure has the following features: The majority of measurements are consistent with noise-only and appear in the large band at the bottom (A). The data composing the horizontal bands (B, C) appear at regular intervals and are consistent with a rotating emitter with its main-lobe coupling into UAVSAR's side lobe. The peak during the middle of the flight line (D) occurs when the emitter is aligned with UAVSAR's main lobe.

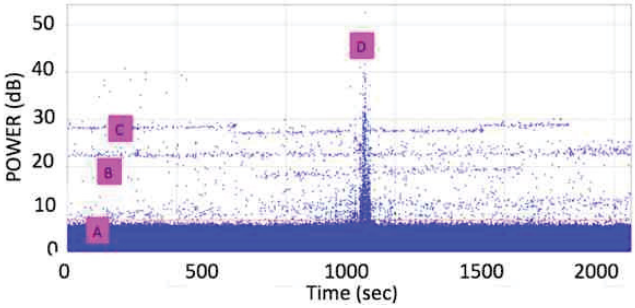

Figure 12 – Pulse-by-pulse power in 1 MHz band for the duration of a UAVSAR flight-line. The labeled feature (A-D) are described in the text.

The data from Figure 12 were combined into a histogram, as shown in Figure 13. This red fit is the expected distribution for Gaussian random noise only, while the blue points are the measured data. The difference between the two are attributable to RFI.

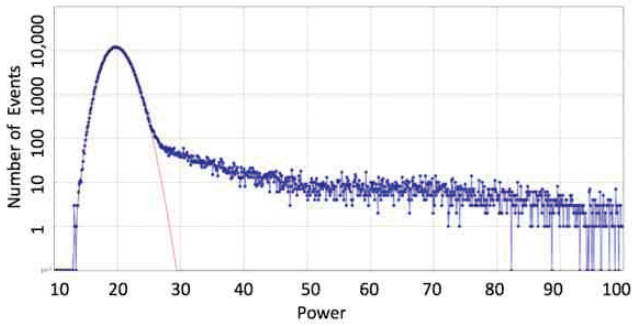

Figure 13 – A histogram of the data from Figure 12 (blue). The red curve is the distribution expected from thermal noise.

The distribution of RFI powers in Figure 13 can be estimated from the convolution of the measured power and the noise-only distribution:

$$H(x) \propto \int_0^x dx' P(x') G(x - x') \qquad (1)$$

There are two knowns: the measured power distribution, *H(x)*, and the noise-only distribution, *G(x)*, which is given by Equation 2 in Appendix II. The one unknown is the RFI-only power distribution, *P(x)*; it relates the two knowns via a convolution given by Equation 1. It may be difficult to invert because of statistical uncertainty and numerical instability at the origin.

Alternatively, a distribution can be chosen and then fit via Monte Carlo methods. That is, random noise data are generated and added to simulated RFI from some model parameterized model distribution; the resulting power distribution is then compared to the observed data. Figure 14 shows the results of such a simulation using a log-normal distribution for P(x), which was chosen because it has been used successfully to model the random nature of signal propagation [11]. The figure demonstrates that this approach describes the data quite well within the statistical limits.

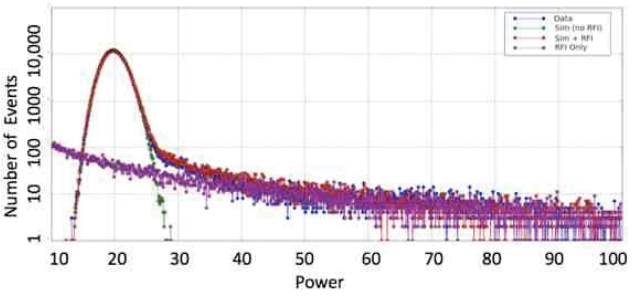

Figure 14 – The blue points are the measured power distribution of 1 MHz bandwidth pulses. The red points are a convolution of the thermal noise distribution (green) and the inferred RFI distribution (magenta). The total RFI power contributing to the peak is only 0.04 dB.

The good agreement between our simulation and the measured data suggests that this approach is a valid methodology for estimating the total RFI power independent of any threshold detection. In other words, it provides a method of estimating contributions from signals falling below detection thresholds.

5. Conclusions

RFI measurements from the PALSAR and UAVSAR sensors have been presented and processed to emulate SMAP's projected high-resolution data product. The results show that RFI needs to be accounted for in order to produce a radiometrically accurate product and that SMAP's baseline algorithm to perform this measurement is technically sound.

The baseline algorithm for SMAP is to threshold-detect pulsed RFI in the raw data product. Regions with RFI will be excised. Estimates from PALSAR data show that the various RFI pulses are infrequent enough that synthetic apertures can almost always be formed, though there are instances where the correct choice of operating frequency will be essential.

The excised range lines will be replaced by an adjacent range line with the appropriate phase noise added. The single-look pixels will be combined into multi-look 3km x 3km pixels. Modeling of this procedure with PALSAR data shows that the RFI contaminated range-lines will spoil the radiometric measurement, though the range-line removal/substitution algorithm presented here can recover the radiometric measurement with a small bias and slight increase in noise that are well within the error budget.

UAVSAR data was used to study the distribution of pulsed RFI noise at one frequency and location. A method for estimating the RFI power distribution for sub-noise power levels was presented and demonstrated with the UAVSAR data. This method can be used to constrain the systematic error on radiometric measurements with pulsed systems.

Finally, a description of the statistics of random measurements in the presence of RFI is presented in Appendix II. The formulae are essential for understanding the probability of false alarm, detection efficiency, and other biases inherent in a threshold detection method.

6. Acknowledgments

This research was carried out at the Jet Propulsion Laboratory, California Institute of Technology for the National Aeronautics and Space Administration.

Appendix I: Continuous Wave Signals In PALSAR

Figure 15 shows a spectrum from PALSAR data. There are several wideband signals with properties consistent with long-range air route surveillance radar and several CW signals.

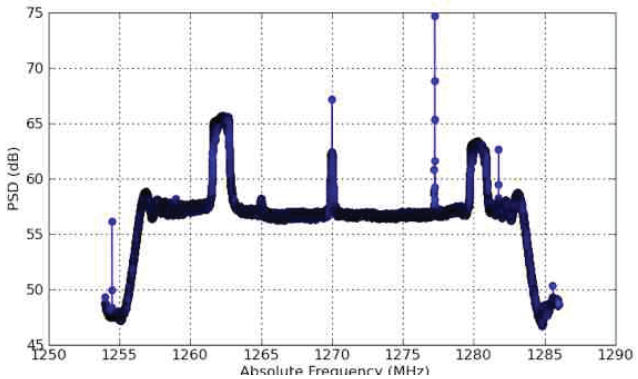

Figure 15 – A PALSAR power spectrum showing continuous wave (CW) signals (narrow spikes) and some wide-band pulsed sources.

The CW signals are easily detected in the frequency domain. The PALSAR data shown can be channelized into 10,304 channels even spaced from 1254 MHz to 1286 MHz. With a PRF of roughly 2.1 kHz, there are about 35,000 pulses in approximately 15 seconds. The total power measured in 4 channels around one of the peaks in Figure 15 is shown in Figure 16. These signals are consistent with amateur radio operations. The peak power in the 3.1 kHz channel is 7-10 dB above the PALSAR signal, but the signal is limited to at most 2 channels so that the ISR over a 1 MHz bandwidth is -15 dB.

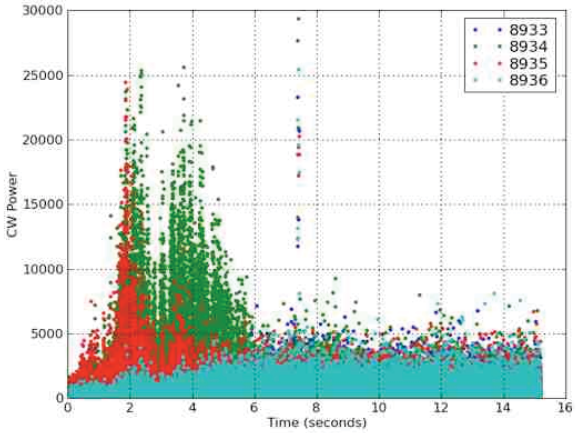

Figure 16 – Channelized total power per pulse for a PALSAR item with CW RFI. The four channels shown span 1281.7422-1281.7516 MHz; the signal is consistent with amateur transmission.

APPENDIX II : STATISTICS OF RADAR MEASUREMENTS WITH RFI

It is well known that coherent radar measurements are distributed according to a 2 dimensional Gaussian distribution, so that the power (the square of the amplitude) is exponentially distributed [10]. Moreover, when incoherently averaging N measurements the distribution becomes a scaled chi-squared distribution with 2N degrees of freedom:

$$p(x) = \frac{N(xN)^{N-1} e^{xN}}{\Gamma(N)} \tag{2}$$

Here the scale factor has been chosen so that the mean value is 1.

The addition of RFI during a single measurement adds an uncorrelated phasor to the 2-dimensional Gaussian distributed measurement. Hence, one look radar backscatter measurement in the presence of RFI can be modeled as a 2-dimensional Gaussian with the mean offset from the origin, with the length, l, of the offset related to RFI power via the Interference-to-Signal Ratio (ISR):

$$l^2 = ISR \tag{3}$$

The distribution of 1 or more Gaussian random variables with non-zero mean is the non-central chi-squared distribution, which a generalization of the standard chi-squared distribution with variables defined by the sum:

$$x = \sum_{i=1}^{k} \left(\frac{X_i - \mu_i}{\sigma_i}\right)^2 \tag{4}$$

where the X_i are k Gaussian random variables with mean μ_i and standard deviation σ_i. A non-central chi-squared distributed variable x is given by:

$$x = \sum_{i=1}^{k} \left(\frac{X_i}{\sigma_i}\right)^2 \tag{5}$$

with the non-centrality parameter λ given by:

$$\lambda = \sum_{i=1}^{k} \left(\frac{\mu_i}{\sigma_i}\right)^2 \tag{6}$$

The probability distribution function (PDF) is then given by $p(x)$ [11]:

$$p(x) = \tfrac{1}{2} e^{-(x+\lambda)/2} \left(\frac{x}{\lambda}\right)^{\frac{k}{4}-\frac{1}{2}} I_{\frac{k}{2}-1}(\sqrt{\lambda x}) \tag{7}$$

where $I_v(z)$ is the modified Bessel function of the first kind. Thus, for multi-looked radar backscatter (N looks) with total RFI power defined by the ISR, the PDF of power measurements is:

$$p(x; N, ISR) = N e^{-N(x+ISR)} \left(\frac{x}{ISR}\right)^{\frac{N-1}{2}} I_{N-1}(2N\sqrt{x(ISR)}) \tag{8}$$

The

distribution is equivalent to the square of the magnitude of a $2N$ dimensional Gaussian random variable offset from the origin by $\lambda^{1/2}$. Since the $2N$-dimensions are orthogonal, and the offset in each dimension is added in quadrature, there is only one non-centrality parameter λ, even though there are k separate μ_i. In other words, the distribution of measurements only depends on the total RFI power in the N measurements, and it does not matter how it is distributed among looks. This fact greatly simplifies the problem of characterizing multi-look measurements with RFI.

The moments of the distribution are:

$$\bar{x} = 1 + ISR$$
$$\sigma = \sqrt{\frac{1+2\,ISR}{N}}$$
$$g_1 = \frac{2(1+3\,ISR)}{\sqrt{N(1+2\,ISR)^3}}$$
$$g_2 = \frac{6}{N}\sqrt{\frac{1+4\,ISR}{(1+2\,ISR)^2}}$$

where g_1 and g_2 are the skewness and kurtosis excess, respectively. Note the first derivative of all the higher moments with respect to the ISR vanish to first order, and are thus not useful in detecting RFI at low levels.

The cumulative distribution function (CDF), $P(x)$, is given by:

$$P(x;N,ISR) = \sum_{j=0}^{\infty} e^{-N\bullet ISR}\frac{(N\bullet ISR)^j}{j!}\frac{\gamma(j+N,Nx)}{\Gamma(j+N)}.$$

In the limit $ISR \rightarrow 0$, this equation contains only the j=0 term and reduces to Equation 2.

Complete and/or incomplete higher-order moments of the distribution are computable from:

$$\left\langle x^m \right\rangle_{x\to\infty} =$$
$$\int_0^x p(t)t^m dt = \sum_{j=0}^{\infty} e^{-N\bullet ISR}\frac{(N\bullet ISR)^j}{j!}\frac{\gamma(j+N+m,Nt)}{\Gamma(j+N)}\Bigg|_{t=0}^{t=x}$$

The incomplete moments can be used to compute means, variances and other moments of measurements with threshold RFI detection—that is, measurements for which data are rejected if they exceed some threshold value.

REFERENCES

[1] "Earth Science and Applications from Space: National Imeratives for the Next Decade and Beyond", Committee on Earth Science and Applications from Space: A Community Assessment and Strategy for the Future, National Research Council, The National Academic Press, 2007. ISBN-10: 0-309-14090-0, ISBN-13: 987-0-309-14090-4.

[2] Soil Moisture Active/Passive (SMAP) Mission NASA Workshop Report, http://science.nasa.gov/media/medialibrary/2010/03/31/Volz1_SMAP_11-20-07.pdf

[3] Hensley, S., *et al.*, 2009. First deformation results using the NASA/JPL UAVSAR instrument, *Proceedings of the 2nd Asian-Pacific Conference on Synthetic Aperture Radar,* 26-30 Oct. 2009, Xian, Shanxi, pp. 1051-1055.

[4] PALSAR User's Guide, 1st Edition, March 2006 Earth Remote Data Analysis Center

[5] Preliminary Draft Revision of Recommendation ITU-R M.1787, "Description of systems and networks in the radionavigation-satellite service (space-to-Earth and space-to-space) and technical characteristics of RNSS transmissions in the bands 1 164-1 215 MHz, 1 215-1 300 MHz,and 1 559-1 610 MHz"

[6] Recommendation ITU-R M.1732, "Characteristics of systems operating in the amateur and amateur-satellite services for use in sharing studies

[7] SF29-22/D "Technical and Operational Characteristics of ALOS-2 SAR" Space Frequency Coordination -29 Meeting, 2009

[8] "Leveraging Multiple FAA Radars for NWS Operations", Michael J. Istok, et al., *25th Conference on International Interactive Information and Processing Systems for Meteorology, Oceanography, and Hydrology*, Phoenix AZ, USA, Amer. Meteor. Soc., 9B.4

[9] Hamazaki, T., "Overview of the Advanced Land Observing Satellite (ALOS): Its Mission Requirements, Sensors, and Satellite System", ISPRS Joint Workshop "Sensors and Mapping from Space 1999", Hanover, Germany, 1999.

[10] Skolnik, Merrill I., *Introduction to Radar Systems*, McGraw-Hill (1st ed., 1962; 2nd ed., 1980; 3rd ed., 2001), ISBN 0-07-066572-9

[11] M. Awad, K. T. Wong[1] & Z. Li, *An Integrative Overview of the Open Literature's Empirical Data on the Indoor Radiowave Channel's Temporal Properties,*[2] IEEE Transactions on Antennas & Propagation, vol. 56, no. 5, pp. 1451-1468, May 2008

[12] Johnson, N. L., Kotz, S., Balakrishnan, N. (1970), *Continuous Univariate Distributions, Volume 2*, Wiley. ISBN 0-471-58494-0

BIOGRAPHY

J. Eric Belz *is a staff engineer in the Radar Science and Engineering section at the Jet Propulsion Laboratory in Pasadena were he was worked on the Shuttle Radar Topography Mission, landing radars for Spirit, Opportunity, and Phoenix. He received his Ph.D. in Physics from the California Institute of Technology in 1994.*

Bryan L. Huneycutt *received the B.S. degree in mathematics from the North Carolina State University at Raleigh in 1969 and the M.S. degree in electrical engineering from the State University of New York at Buffalo in 1975. He has worked at the Cornell Aeronautical Laboratory (Calspan) in Buffalo, NY on radar target classification and radar system modeling for parameter tradeoff studies from 1969 to 1974. In 1974, he joined the Telecommunications Science and Engineering Division of the Jet Propulsion Laboratory, Pasadena, CA. He first worked on the Viking Project in software engineering and operations support for the Viking Orbiter communications system. He has worked on the SEASAT SAR program in the area of the S-band data link for the SAR. He was systems engineer for the Shuttle Imaging Radar-A (SIR-A) which flew in 1981 and he was the instrument engineer for SIR-B which flew in 1984 He was supervisor of the SIR-C RF Electronics group and the Deputy System Manager for the Spaceborne Imaging Radar-C (SIR-C) which flew in 1994. Since 1996 he has been involved in system design and modeling of synthetic aperture radars. He supported the system engineering studies for LightSAR, the AFRL/JPL Space-based Radar, Ocean Observer SAR, etc. He was cognizant engineer for the radar altimeter which flew on the lander of the Mars Pathfinder which landed on Mars on July 4, 1997 and is presently involved in system engineering studies concerning RFI for the Soil Moisture Active/Passive radar. Since 1994, he has been the ITU-R remote sensing representative for NASA/JPL and US delegate at international meetings of the ITU-R in Geneva, Switzerland, and Space Frequency Coordination Group meetings to ensure availability and protection of frequency spectrum for NASA active spaceborne sensors.*

Michael Spencer *came to JPL in 1990 and initially worked on modeling and simulation for the NASA scatterometer (NSCAT) instrument, a Ku-band radar launched in 1996 to measure sea-surface winds from space. He was involved as a lead systems engineer for the SeaWinds instrument (a follow-on to NSCAT) from the early conceptual design phase through launch, calibration, and operations on the QuikSCAT satellite in 1999 and again on the ADEOS-2 satellite in 2002. He continues to be interested in wind sensing from space, and has developed concepts for future high-resolution systems. More recently, Dr. Spencer has been lead payload system engineer for the development of an advanced radar for the measurement of soil moisture. For the Soil Moisture Active/Passive (SMAP) mission, he has been responsible for the design of a unique L-band synthetic aperture radar (SAR), which utilizes a large rotating mesh reflector antenna to achieve a very wide measurement swath.*